Three Novel Zintl Phases in the Mg–La–Sb System Based on Intergrowth of LaSb and Mg_3Sb_2 Slabs

Ashok K. Ganguli, Young-Uk Kwon, and John D. Corbett*

Ames Laboratory—DOE[1] and Department of Chemistry, Iowa State University, Ames, Iowa 50011

Received March 31, 1993®

Reactions of the elements in welded Ta containers at 875–1050 °C produce the black brittle compounds $Mg_{4.5}La_4Sb_7$ (5-4-7), $Mg_{4.6}La_3Sb_6$ (5-3-6), and $Mg_{1.7}La_{4.9}Sb_6$ (2-5-6). All three consist of coherent intergrowths of Mg_5Sb_4 (in 5-4-7 and 5-3-6) or Mg_2Sb_2 (2-5-6) slabs derived from Mg_3Sb_2 (3-0-2) (anti-α-La_2O_3) with $La_{n+1}Sb_n$ slabs from LaSb (NaCl-type) for n = 3, 2, and 4, respectively, in which a layer of (111) La replaces octahedral (001) Mg at the interface. Crystal data for 5-4-7, 5-3-6, 2-5-6, 3-0-2, respectively, are as follows. Space group, Z: $P\bar{3}m1$, 1; $R\bar{3}m$, 3; $R\bar{3}m$, 3; $P\bar{3}m1$, 1. a = 4.6206(5), 4.615(1), 4.616(1), 4.559(1) Å; c = 26.069(7), 66.91(2), 67.67(4), 7.243(2) Å. No. of independent data, variables: 338, 29; 272, 26; 144, 20; 107, 10. R/R_w (%): 3.0, 3.4; 2.4, 2.8; 2.2, 2.6; 1.5, 2.4. The refined deficiencies at Mg sites, and at the La interface in 2-5-6 as well, result from the above interfacial substitution and are in amounts necessary to afford valence (Zintl) compounds for all three. The 5-4-7, 2-5-6, and 3-0-2 compounds are diamagnetic and show temperature-independent resistivities of the order of 50, 85, and 530 $\mu\Omega$·cm, respectively. Semi-metal behaviors are consistent with this property of bulk LaSb, the intergrowth structures, and Zintl phase concepts. Possibilities for the formation of analogous intergrowth compounds in other systems are suggested.

Introduction

Binary and ternary phases composed of main-group elements from the silicon, arsenic, and sulfur families combined with electropositive metals constitute a large fraction of what have been described as Zintl (valence) phases, some of considerable beauty, variety, and complexity.[2] Our explorations of mainly electron-rich compounds, particularly those formed between Ge, Sn, or Pb and Zr, La, Ca, Sr, or Ba, have also demonstrated how some of these can be converted to Zintl phases with the introduction of electronically suitable interstitials.[3-7] The impetus for the present investigation was note of the fact that very little information about ternary Zintl phases of the lanthanide elements has been published. A Zintl formulation appears to apply to a few reported binary phases for rare-earth–main-group elements.[8] The most positive results are found with the main-group elements with high electronegativity. The pnictides LaP_2 (P_3^{5-} and P_3^{7-} chains)[9] and LaP_5 (2-D nets with 12-membered rings of 3-bonded (3b)P^0 and 2b-P^+)[10] and the monopnictides LaP, LaAs, and LaSb (rock-salt)[11] are all Zintl phases to the first approximation although confirmatory property data have not been reported for the first two. Other phases in the La–Sb binary system [La_2Sb, $LaSb_2$ ($SmSb_2$-type), and La_4Sb_3 (anti-Th_3P_4)][8] do not fit into the Zintl–Klemm picture. The monochalcogenides (LaS, LaSe, and LaTe; all rock-salt) are well-known to be metallic by virtue of one extra electron per formula unit, but the status of the dichalcogenides (LaS_2, $LaSe_2$, and $LaTe_2$; Cu_2Sb-type)[11] is unclear. Within the Mg–La–Sb system we have studied, the only other meaningful binary, Mg_3Sb_2, is a classical example of a Zintl phase that was first studied by Zintl himself.[12] He reported it to have the inverse α-La_2O_3 structure, although no positional refinements have been reported.

One incentive for the investigation of ternary compounds with magnesium stemmed from the fact that lithium forms many ternaries with rare-earth and main-group elements like Li_3LaP_2, Li_3LaSb_2, and $LiLaSn_2$,[13,14] and the long-known diagonal relationship with magnesium would suggest a possibly comparable behavior there. In this report we present the syntheses, crystal structures, and magnetic, conduction, and XPS properties of three novel Zintl phases with the compositions $Mg_{4.5}La_4Sb_7$ (5-4-7), $Mg_{4.6}La_3Sb_6$ (5-3-6), and $Mg_{1.7}La_{4.9}Sb_6$ (2-5-6). The (idealized) number sets in parenthese will often be used in the text to refer to the corresponding phases. We also report a single-crystal investigation of Mg_3Sb_2 and its magnetic and conduction behavior for comparison.

Experimental Section

Syntheses. All of these phases were synthesized by starting with the pure elements: Mg turnings and La bar (99.99%, Ames Laboratory); Sb shot (99.99%, Aesar). The metals were stored and handled in a helium-filled glovebox. The surface of the La was scaped off before use. Stoichiometric amounts of the elements were loaded into Ta tubes. These were welded under helium atmosphere and in turn jacketed within fused silica containers that were well flamed under high vacuum prior to sealing in order to remove as much moisture from the glass as possible. For the synthesis of Mg_3Sb_2, 5-4-7, and 5-3-6 the assembly was heated in a resistance furnace at 870 °C for 15 d and then slowly cooled. (The rate does not seem important.) Mg_3Sb_2 and 5-4-7 could be obtained as single phases (to X-rays) by this method, while the 5-3-6 composition also contained 5-4-7 and Mg_3Sb_2 (~40% each). A single-phase sample of 2-5-6 was prepared by reaction at 1050 °C for 3 d followed by quenching. All samples were opened in a nitrogen-filled glovebox to avoid moisture

* Abstract published in *Advance ACS Abstracts*, September 1, 1993.
(1) Ames Laboratory is operated for U.S. Department of Energy by Iowa State University under Contract No. W-7405-Eng-82. This research was supported by the Office of the Basic Energy Sciences, Materials Sciences Division, DOE.
(2) Schäfer, H. *Annu. Rev. Mater. Sci.* **1985**, *15*, 1.
(3) Hurng, W.-M.; Corbett, J. D. *Chem. Mater.* **1989**, *1*, 311.
(4) Kwon, Y.-U.; Corbett, J. D. *Chem. Mater.* **1992**, *4*, 1348.
(5) Guloy, A. M.; Corbett, J. D. *Z. Anorg. Allg. Chem.* **1992**, *616*, 61.
(6) Guloy, A. M.; Corbett, J. D. *Inorg. Chem.* **1993**, *32*, 3532.
(7) Guloy, A. M. Ph.D. Dissertation, Iowa State University, 1992.
(8) *Binary Alloy Phase Diagrams*, 2nd ed.; Massalski, T., Ed.; American Society for Metals International: Metals Park, OH, 1990; p. 954.
(9) von Schnering, H.-G.; Wichelhaus, W.; Nahrup, M. S. *Z. Anorg. Allg. Chem.* **1975**, *412*, 193.
(10) Wichelhaus, W.; von Schnering, H.-G. *Z. Anorg. Allg. Chem.* **1976**, *419*, 77.
(11) Villars, P.; Calvert, L. D. *Pearson's Handbook of Crystallographic Data for Intermetallic Phases*, 2nd ed.; American Society for Metals International: Metals Park, OH, 1991.
(12) Zintl, E.; Husemann, E. *Z. Phys. Chem.* **1933**, *21B*, 138.
(13) Grund, I.; Schuster, H.-U.; Müller, P. *Z. Anorg. Allg. Chem.* **1984**, *515*, 151.
(14) Pavlyuk, V. V.; Bodak, O. I.; Pecharskii, V. K.; Skolodra, R. V.; Gladyshevskii, E. I. *Inorg. Mater.* **1989**, *25*, 962.

0020-1669/93/1332-4354$04.00/0

Table I. Selected Crystallographic and Refinement Details

	Mg_3Sb_2	$Mg_{4.47(5)}La_4Sb_7$	$Mg_{4.61(7)}La_3Sb_6$	$Mg_{1.66(6)}La_{4.89(2)}Sb_6$
lattice params,[a] Å	a = 4.559(1)	a = 4.6206(5)[b]	a = 4.615(1)	a = 4.616(1)
	c = 7.243(2)	c = 26.069(7)	c = 66.91(2)[b]	c = 67.67(4)
space group, Z	$P\bar{3}m1$ (No. 164), 1	$P\bar{3}m1$ (No. 164), 1	$R\bar{3}m$ (No. 166), 3	$R\bar{3}m$ (No. 166), 3
μ, cm^{-1} (Mo Kα)	106.1	185.2	175.4	220.5
transm coeff range	0.822–1.045	0.921–1.177	0.338–1.00	0.938–1.118
no. of indep obs refl, variables	107, 10	338, 29	272, 26	144, 20
R, R_w[c]	0.015, 0.024	0.030, 0.034	0.024, 0.028	0.022, 0.026

[a] Guinier data unless noted otherwise; λ = 1.540 562 Å. [b] CAD-4 data. [c] $R = \sum||F_o| - |F_c||/\sum|F_o|$; $R_w = [\sum w(|F_o| - |F_c|)^2/\sum w(F_o)^2]^{1/2}$; $w = \sigma_F^{-2}$.

and oxygen. Even so, the bulk compounds visually seem to be stable in the air for days or weeks, and no changes were observed in the powder patterns of 5-4-7 and 2-5-6 after 3 d in air.

X-ray Powder Diffraction. Powder patterns were obtained for samples mounted between pieces of cellophane tape. An Enraf-Nonius Guinier camera, Cu Kα_1 radiation, and NBS (NIST) silicon as internal standard were employed for this purpose. The known 2θ values of the standard lines were fitted to a quadratic in their position on the film, and lattice constants of the sample were then calculated by a least-squares fit to 2θ values after the structure determination allowed indexing.

Properties. Magnetic susceptibility samples were held between two silica rods within a closely fitting silica tube. The assembly was evacuated, back-filled with helium, and sealed. The susceptibilities were measured at 3 T over the range 6–298 K on a Quantum Design SQUID magnetometer. The raw data were corrected for the susceptibility of the container and the diamagnetic susceptibilities of the ion cores. Conductivities of sized samples of three compounds mixed with chromatographic Al_2O_3 were measured by the "Q" method[15] at 35 MHz. Room-temperature XPS data were acquired for 5-4-7 and 2-5-6 samples with the aid of a Physical Electronics Industries 5500 surface analysis system. Monochromatic Al Kα radiation (1486.6 eV) at 300 W was used for excitation. A significant oxide layer on the surfaces of the samples was evident by this means.

Crystal Structures. Mg_3Sb_2. The refinement of this structure with 107 independent reflections from a Rigaku AFC6R diffractometer in the reported inverse α-La_2O_3 structure type ($P\bar{3}m1$, Z = 1) proceeded smoothly to R/R_w = 0.015, 0.024 (Table I). The largest residual, 0.8 e/Å^3, was 0.54 Å from Mg1. The lattice parameters are within ~0.01 Å of those reported by Zintl,[12] while the fractional coordinate values extend those he assumed by two significant figures.

$Mg_{4.5}La_4Sb_7$ (5-4-7). A black platelike crystal with dimensions 0.25 × 0.15 × 0.06 mm was mounted within a glass capillary in a glovebox. The crystal was first checked by oscillation photographs and then transferred to an automatic diffractometer (Enraf-Nonius CAD-4) for data collection at room temperature with monochromated Mo Kα radiation. Selected parameters for the data collection and refinement are listed in Table I. The diffraction data were corrected for Lorentz and polarization effects and for absorption using the average of three ψ scans at different θ values. An empirical absorption correction using DIFABS[16] was later applied before the anisotropic refinement.

The centrosymmetric space group $P\bar{3}m1$ was chosen for the trial structure solution on the basis of absence of systematic extinctions, the $N(Z)$ centricity test, and the indicated Laue group. Application of direct methods (SHELXS[17]) did not provide a satisfactory model, but a model that refined smoothly was obtained when the space group symmetry was lower to $P3m1$. That many of the positions were related by an inversion center became evident after a few cycles of least-squares refinement and the calculation of a different Fourier map. The refinement proceeded smoothly with all nine positions fully occupied when the symmetry was returned to that of $P\bar{3}m1$. However, the thermal parameters of Mg1, Mg3, and Sb4 appeared to be larger than those of other similar atoms in the structure. The occupancy of Sb4 remained within 3σ of 100% when varied, while simultaneous variation of the occupancies of Mg1 and Mg3 (isotropic) smoothly refined to 82(3)% and 83(2)%, respectively. The final least-squares cycles involved all positional and anisotropic thermal parameters, occupancies of these two Mg atoms, and a secondary extinction coefficient. The refined composition is $Mg_{4.47(5)}La_4Sb_7$. The largest residua, 2.99 e/Å^3, was 1.31 Å from Mg3 at $^2/_3$, $^1/_3$, 0.047. All the calculations were carried out with the TEXSAN package.[18]

$Mg_{4.6}La_3Sb_6$ (5-3-6). A black platelike crystal was first checked by oscillation methods and then mounted on a CAD-4 automatic diffractometer for further studies. The random search and indexing procedure led to a C-centered monoclinic cell, with a = 7.994(1) Å, b = 4.614(1) Å, c = 22.457(5) Å, and β = 96.83(2)°. Data collected on the basis of this cell and the absence of other extinctions indicated possible space groups $C2$, Cm, and $C2/m$. Direct methods eventually led to a reasonable model in Cm with all atoms and low residuals but at the cost of unreasonable anisotropic thermal parameters and some high correlation coefficients. Transformation of the data to the alternate rhombohedral (hexagonal) $R\bar{3}m$ also indicated by the initial orientation on the diffractometer allowed all eight atoms to be located and refined well, and the resultant difference Fourier map was nearly flat. Only the occupancies of two Mg atoms refined to less than 100% (Mg2, 90(3)%; Mg1, 80(4)%). Final refinement of all the positional and anisotropic thermal parameters, a secondary extinction correction, and the two occupancies led to reasonable results. The refined composition is $Mg_{4.61(7)}La_3Sb_6$. The largest residual, 2.46 e/Å^3, was 1.30 Å from Mg2.

$Mg_{1.7}La_{4.90}Sb_6$ (2-5-6). Oscillation and Weissenberg photographs of a small black platelike crystal suggested a rhombohedral space group with a ~ 4.61 Å and c ~ n(22.5) Å. Twenty-five reflections located by a random search on a CAD-4 diffractometer were subsequently refined and indexed on a hexagonal cell with a = 4.614(1) Å and c = 67.58(1) Å. The Laue check suggested trigonal symmetry and a possible R centering. Systematic absences, apparently equivalent sets of reflections, and the centric statistics indicated the $R\bar{3}m$ space group. Direct methods[17] again gave a satisfactory model, the heavy atoms being assigned as either Sb or La on the basis of reasonable bond distances. Least-squares refinements and difference Fourier syntheses revealed all atoms. Refinement of occupancies at this stage (R = 3.9%) led to marginal partial occupancies for the Mg and La3 atoms. An additional absorption correction (DIFABS[16]) was applied before the anisotropic refinement (R_{av} = 0.044, $I > 0$). The final refinement of all the positional and anisotropic thermal parameters (and an isotropic parameter for Mg) and the two occupancies led to a R/R_w of 0.020/0.021. The refined composition was $Mg_{1.7(1)}La_{4.90(2)}Sb_6$. Because of the small data set, the structure of another crystal from the same reaction was refined with 23% more observed reflections collected on a Rigaku AFC6R diffractometer. The refinement outcome was very close to the previous result and confirmed the partial occupancies of both the Mg sites and one La site, giving the composition $Mg_{1.66(6)}La_{4.89(2)}Sb_6$. The standard deviations of the parameters and the sizes of the ellipsoids were all smaller with the second crystal, and so these are the data reported.

Results and Discussion

The three new Mg–La–Sb phases are all constructed from alternating slabs of two basic building blocks that derive from two valence compounds, Mg_3Sb_2 (anti-α-La_2O_3) and LaSb (rock-salt). The structures differ among one another primarily in the type of the Mg_3Sb_2-based slabs utilized and in the number of rock-salt-type LaSb layers intergrown between these. The c parameters naturally depend on the type of intergrowth (Table I), while the a values of the three structures are very similar (4.615(1)–4.6206(5) Å) and slightly larger than a for Mg_3Sb_2 (4.559(1) Å) and $a/\sqrt{2}$ of LaSb (4.589 Å).[19] A single-crystal

(15) Shinar, J.; Dehner, B.; Beaudry, B. J.; Peterson, D. T. *Phys. Rev.* **1988**, *B37*, 2066.
(16) Walker, N.; Stuart, D. *Acta Crystallogr.* **1983**, *A39*, 158.
(17) Sheldrick, G. M. SHELXS-86. Universität Göttingen, BRD, 1986.
(18) TEXSAN, version 6.0 package. Molecular Structure Corp., The Woodlands, TX, 1990.
(19) Leger, J. M.; Ravot, R. D.; Rossat-Mignod, J. *J. Phys. C.: Solid State Phys.* **1984**, *17*, 4935.

Table II. Positional and Isotropic-Equivalent Thermal Parameters[a] for the Four Structures

atom	x	y	z	B_{eq}	occ
			Mg_3Sb_2		
Sb	1/3	2/3	0.22982(7)	1.38(3)	
Mg1	0	0	0	1.0(1)	
Mg2	1/3	2/3	0.6361(5)	1.87(9)	
			$Mg_{4.5}La_4Sb_7$		
La1	1/3	2/3	0.42959(3)	0.80(3)	1
La2	0	0	0.28827(4)	0.89(3)	1
Sb1	0	0	1/2	0.82(4)	1
Sb2	2/3	1/3	0.35691(4)	0.85(3)	1
Sb3	1/3	2/3	0.21246(5)	0.99(3)	1
Sb4	2/3	1/3	0.06417(5)	1.53(3)	1
Mg1	0	0	0	2.2(4)	0.82(3)
Mg2	2/3	1/3	0.1733(3)	1.7(2)	1
Mg3	1/3	2/3	0.0969(3)	2.0(2)	0.83(2)
			$Mg_{4.6}La_3Sb_6$		
La1	1/3	2/3	1/6	0.69(4)	1
La2	0	0	0.11205(2)	0.77(3)	1
Sb1	2/3	1/3	0.13883(2)	0.70(3)	1
Sb2	1/3	2/3	0.08263(2)	0.87(2)	1
Sb3	2/3	1/3	0.02487(2)	1.42(3)	1
Mg1	0	0	0	1.9(4)	0.80(4)
Mg2	1/3	2/3	0.0374(1)	2.5(3)	0.90(3)
Mg3	2/3	1/3	0.0674(1)	1.4(2)	1
			$Mg_{1.7}La_{4.9}Sb_6$		
La1	0	0	0	0.5(1)	1
La2	2/3	1/3	0.0564(4)	0.66(8)	1
La3	1/3	2/3	0.10933(4)	0.7(1)	0.945(8)
Sb1	1/3	2/3	0.0754(4)	0.9(1)	1
Sb2	0	0	0.08289(4)	0.8(1)	1
Sb3	2/3	1/3	0.13824(4)	0.9(1)	1
Mg	0	0	0.1523(3)	0.9(3)	0.83(3)

[a] $B_{eq} = (8\pi^2/3)\sum_i\sum_j U_{ij}a_i^*a_j^*\tilde{a}_i\tilde{a}_j$.

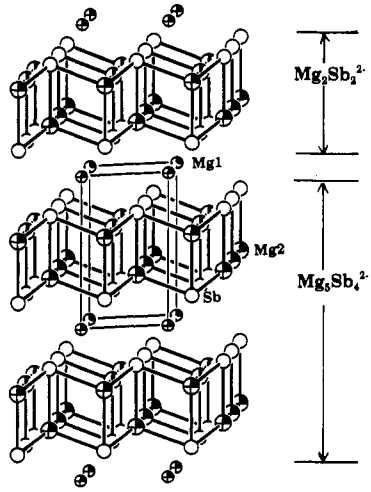

Figure 1. ~[100] view of the structure of Mg_3Sb_2 with the unit cell outlined. The $Mg_2Sb_2^{2-}$ and $Mg_5Sb_4^{2-}$ slabs found in intergrowth are indicated. Shaded and open (94%) ellipsoids are Mg and Sb atoms, respectively. Bonds to the Mg1 atoms between the bilayers have been omitted.

study of Mg_3Sb_2 was also carried out in order to gain better bond distance data for a closer comparison with these new structures. Selected data collection and refinement parameters were given in Table I, and the positional and isotropic-equivalent thermal parameters for all four structures are given in Table II. Distances appear in Table III.

Mg_3Sb_2. This structure, the anti-type of α-La_2O_3, can be described in terms of hcp Sb layers between which magnesium occupies half of the octahedral and half of the tetrahedral interstices in an ordered way, namely, Mg1 in all octahedral (trigonal antiprismatic) sites between one pair of layers (AB) and Mg2 in all the tetrahedral interstices between the other pair (BA), viz. AcBabA... (or as NaCl and CaF_2 intergrown at the layer level). A useful way of looking at this structure (Figure 1) is in terms of puckered $\bar{3}m1$ $^2_\infty[Mg_2Sb_2^{2-}]$ bilayers containing tetrahedral Mg ions that are stacked along $\vec{c}$ with the same orientation and separated by layers of Mg^{2+} in the octahedral sites. (This will also be recognized as the isostructural $CaAl_2Si_2$[20] where Ca and Al replace Mg1 and Mg2, respectively.) The indicated $^2_\infty[Mg_5Sb_4^{2-}]$ building block contains two bilayered units plus one intervening layer of octahedral Mg^{2+} ions. The flexibility of the Mg_3Sb_2 structure in forming intergrowth structures can be ascribed in part to the ease of substitution of La for these octahedral Mg atoms, which have longer and perhaps weaker Mg–Sb bonds (3.11 Å) compared with the tetrahedrally oriented Mg–Sb (2.81–2.94 Å) within the $Mg_2Sb_2^{2-}$ bilayers. In the three intergrowth structures 5-4-7, 5-3-6, and 2-5-6 that follow, the interfaces between the bilayers from Mg_3Sb_2 and the slabs from cubic LaSb involve substitution of one extra layer of La atoms for the octahedral Mg1 members in the Mg_3Sb_2 portion.

$Mg_{4.5}La_4Sb_7$. The 5-4-7 structure shown in Figure 2 can be seen to consist of the former $Mg_5Sb_4^{2-}$ units (now $Mg_{4.5}Sb_4^{3-}$ with vacancies, below) interleaved with four close-packed (111) metal and three metalloid layers from cubic LaSb, viz., $La_4Sb_3^{3+}$. The latter lie horizontal in the figure. The intergrowth is thus between (111) LaSb and (001) Mg_3Sb_2. (The orientation of the next layer in the Mg_3Sb_2 portion, Sb3, matches the preceding LaSb portion, but these atoms have a different coordination number (3 + 3 + 1).) The *a* repeats in the separate blocks, 4.589 and 4.559 Å, respectively, become 4.621 Å when intergrown. Actually, distortions in the pair of bilayers, which have now $3m1$ symmetry, are more substantial with the substitution of La2 on one side. The umbrella arrangement about Sb3 distorts more with the new La neighbors, while that about the interior Sb4 becomes more symmetric. Contrarywise, the tetrahedra about Mg2 and Mg3 (interior) become more and less uniform, respectively. The LaSb layers now contain slightly distorted octahedra with three short and three long bonds (Table III) within

Table III. Bond Distances in the Four Structures (Å)

			Mg_3Sb_2		
Mg1–Sb	×6	3.1143(6)	Sb–Mg1	×3	3.1143(6)
Mg2–Sb	×3	2.806(2)	Sb–Mg2	×3	2.806(2)
Mg2–Sb	×1	2.943(4)	Sb–Mg2	×1	2.943(4)
			$Mg_{4.5}La_4Sb_7$		
Mg1–Sb4	×6	3.1488(8)	Sb1–La1	×6	3.2382(6)
Mg2–Sb3	×3	2.857(2)	Sb2–La1	×3	3.2721(6)
Mg2–Sb4	×1	2.844(7)	Sb2–La2	×3	3.2123(9)
Mg3–Sb3	×1	3.014(9)	Sb3–La2	×3	3.320(1)
Mg3–Sb4	×3	2.801(3)	Sb3–Mg2	×3	2.857(2)
La1–Sb1	×3	3.2382(6)	Sb3–Mg3	×1	3.014(9)
La1–Sb2	×3	3.2721(6)	Sb4–Mg1	×3	3.1488(8)
La2–Sb2	×3	3.2123(9)	Sb4–Mg2	×1	2.844(7)
La2–Sb3	×3	3.320(1)	Sb4–Mg3	×3	2.801(3)
			$Mg_{4.6}La_3Sb_6$		
Mg1–Sb3	×6	3.142(1)	Sb1–La1	×3	3.2511(9)
Mg2–Sb2	×1	3.03(1)	Sb1–La2	×3	3.211(1)
Mg2–Sb3	×3	2.793(3)	Sb2–La2	×3	3.313(1)
Mg3–Sb2	×3	2.853(2)	Sb2–Mg3	×3	2.853(2)
Mg3–Sb3	×1	2.844(6)	Sb2–Mg2	×1	3.03(1)
La1–Sb1	×6	3.2511(9)	Sb3–Mg1	×3	3.142(1)
La2–Sb1	×3	3.211(1)	Sb3–Mg2	×3	2.793(1)
La2–Sb2	×3	3.313(1)	Sb3–Mg3	×1	2.844(6)
			$Mg_{1.7}La_{4.9}Sb_6$		
Mg–Sb3	×1	2.90(2)	Sb1–La1	×3	3.252(2)
Mg–Sb3	×3	2.829(6)	Sb1–La2	×3	3.235(3)
La1–Sb1	×6	3.252(2)	Sb2–La2	×3	3.280(3)
La2–Sb1	×3	3.235(3)	Sb2–La3	×3	3.210(3)
La2–Sb2	×3	3.280(3)	Sb3–Mg	×1	2.90(2)
La3–Sb2	×3	3.210(3)	Sb3–Mg	×3	2.829(6)
La3–Sb3	×3	3.306(3)	Sb3–La3	×3	3.306(3)

(20) Gladyshevskii, E. I.; Kripyakevich, P. I.; Bodak, O. I. *Ukr. Fiz. Zh. (Russ. Ed.)* **1967**, *12*, 447.

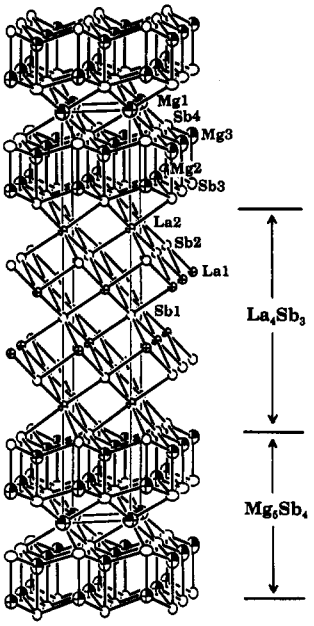

Figure 2. Structure of the $Mg_{4.5}La_4Sb_7$ (5-4-7) phase viewed along ~-[100] with the unit cell outlined. Shaded, crossed, and open ellipsoids (94%) represent Mg, La, and Sb atoms, respectively. Note the intergrowth of La_4Sb_3 (NaCl) layers (horizontal) with Mg_5Sb_4 slabs (Figure 1). Magnesium vacancies are present in the latter.

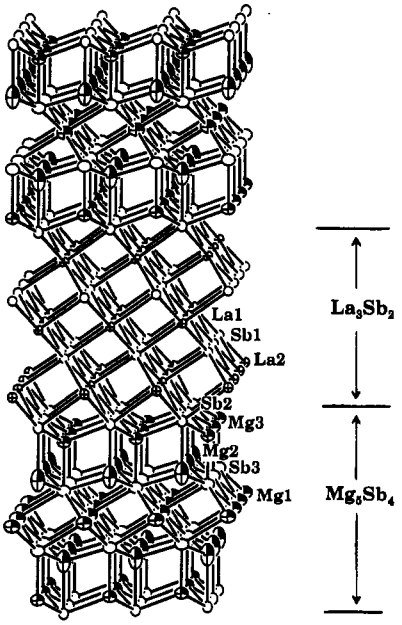

Figure 3. The independent one-third of the rhombohedral structure of $Mg_{4.6}La_3Sb_6$ viewed along ~[100] ($\vec{c}$ vertical). Shaded, crossed, and open ellipsoids represent Mg, La, and Sb atoms, respectively. Note the intergrowth of La_3Sb_2 (111) and Mg_5Sb_4 (001) slabs.

the range 3.212–3.272 Å (except for La2–Sb3 at the interface which is longer, 3.320 Å), comparable to those in LaSb (3.245 Å). The relatively large thermal parameter for Sb4 (Table II, Figure 2), although not particularly unusual compared with that in Mg_3Sb_2, probably arises from the fact that six of the seven neighboring Mg sites are ~80% occupied (Mg1, Mg2). The structure can also be described in terms of pairs of substituted $CaAl_2Si_2$-type units $MgLa(Mg_2Sb_2)_2$ with some Mg defects that are intergrown with La_3Sb_3.

$Mg_{4.6}La_3Sb_6$. The structure is closely related to that of $Mg_{4.5}La_4Sb_7$ (5-4-7), although it crystallizes in the rhombohedral instead of a primitive trigonal cell. In Figure 3 we show (approximately) the independent one-third of the cell along the 66.9-Å c axis. Here three La and two Sb layers from LaSb

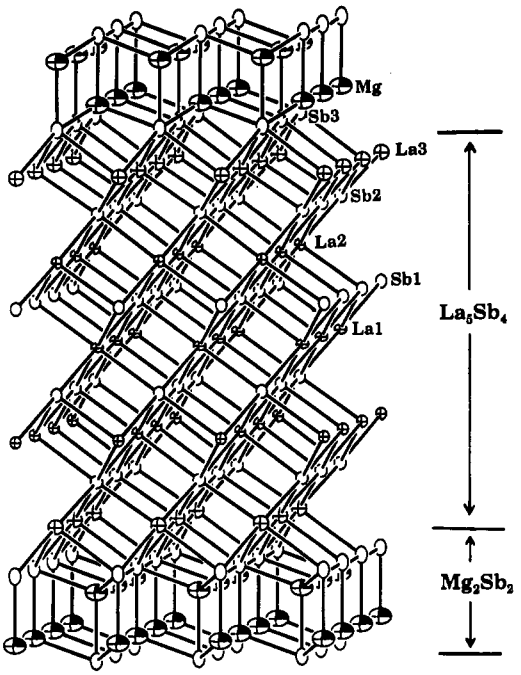

Figure 4. One-third of the $Mg_{1.7}La_{4.9}Sb_6$ structure along ~[100]. Shaded, crossed, and open ellipsoids represent Mg, La, and Sb atoms, respectively. The intergrowth is between La_5Sb_4 and Mg_2Sb_2 units.

(instead of four and three before) alternate with double blocks of $Mg_{4.5}Sb_4^{3-}$. The decrease in the number of (111) La layers from 4 to 3 means neighboring $Mg_5Sb_4^{2-}$ slabs are staggered rather than eclipsed as they were in the 5-4-7 structure, and a rhombohedral stacking results. Two of the metal sites in each $Mg_5Sb_4^{2-}$ block are partially occupied, very similar to the disposition found in the 5-4-7 phase. The bond lengths (Table III) are also comparable. The two tetrahedrally-coordinated Mg atoms have similar features as in the 5-4-7 structure, the exterior one (Mg3) having four nearly equal Mg–Sb bonds while the other has one longer (3.03 Å) and three equal (2.79 Å) Mg–Sb bonds. The thermal parameter of the Sb3 atom, which is bound in the main part to the fractional Mg atoms, is again larger, as it was for the analogous Sb4 in 5-4-7. The La–Sb distances in the rock-salt layers vary from 3.211 to 3.313 Å (Table III), very similar to those in the 5-4-7 structure.

$Mg_{1.7}La_{4.9}Sb_6$. The structure of 2-5-6 (Figure 4) involves a closely related arrangement, single (defect) $Mg_2Sb_2^{2-}$ slabs interleaved with five (111) lanthanum and four antimony layers from LaSb (nominally $La_5Sb_4^{3+}$) along $\vec{c}$. Neighboring $Mg_2Sb_2^{2-}$ slabs have different projections, again leading to a long rhombohedral sequence repeat rather than the shorter cell in 5-4-7. Figure 5 shows the entire cells for 2-5-6 and 5-3-6 in a more schematic view to emphasize the differences in their structures. The powder patterns of 5-3-6 and 2-5-6 are easily distinguishable, while the pattern of 5-3-6 is quite similar to that of 5-4-7. The single $Mg_2Sb_2^{2-}$ slabs again have $\bar{3}m1$ symmetry, and the octahedral Mg atoms present in the other structures are now absent. The tetrahedral (and only) Mg site is ~83% partially occupied as before, but the La site in the interface with the bilayer also has a slight (7σ) deficiency, presumably driven by charge balance constraints (below). The Mg–Sb and La–Sb distances are comparable to those found in the other intergrowth structures. The Sb3 atoms in the bilayers now have mixed metals in their monocapped antiprismatic environments and exhibit smaller and less distinctive ellipsoids (Table II), presumably because the La3 defect on one side is notably less than those around Sb4 in 5-4-7 and Sb3 in 5-3-6.

Properties. The small cation deficiencies found in all the above compounds seem to be driven by electronic considerations, namely, the balance of charge differences that would otherwise arise at

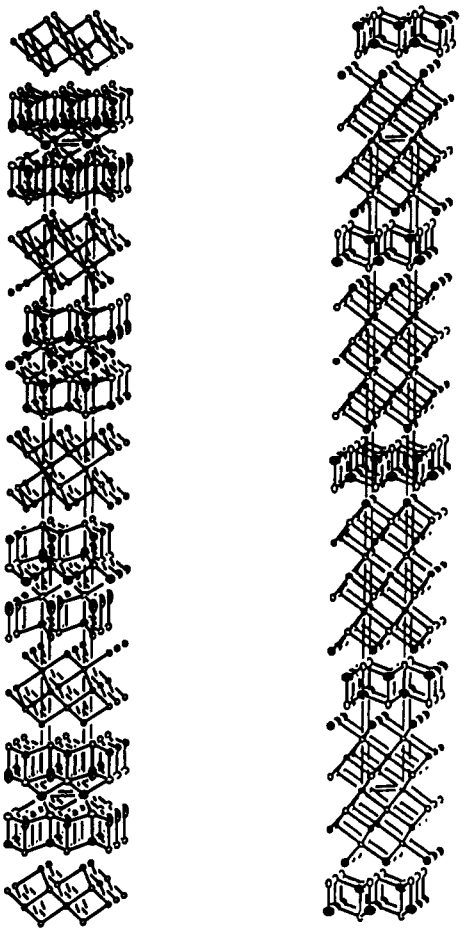

Figure 5. Full cells of (left) $Mg_{4.6}La_3Sb_6$ (5-3-6) and (right) $Mg_{1.7}La_{4.9}Sb_6$ (2-5-6) viewed approximately along [100].

the slab interfaces where La^{3+} substitutes for Mg^{2+}. These defects occur only in the inner regions of the Mg_5Sb_4 slabs in 5-4-7 and 5-3-6, making each very close to $Mg_{4.5}Sb_4^{3-}$, but they also occur to a small degree (5.5(8)%) at the interfacial La3 atom in 2-5-6, where only single $Mg_{1.66}Sb_2$ bilayers are present. The refined compositions of the three intergrowth structures 5-4-7, 5-3-6, and 2-5-6 in fact are charge-neutral within 0.4, 1.5, and 0.1 standard deviations, respectively. Possible alternatives would appear to be some reduction of the cations/occupation of the conduction band or injection of interstitial Sb^{3-}. We have also attempted to vary the magnesium content in $Mg_{5-x}La_4Sb_7$ ($0.0 \leq x \leq 1.0$), but significant variations in lattice constants, usually a good diagnostic for nonstoichiometry, were not found. The character of the structures and the large polarity (valence energy) differences between antimony and the two active metals make it unlikely.

Properties of several of the phases are fairly consistent with our conclusions regarding Zintl phases. Magnetic susceptibility studies show that Mg_3Sb_2, 5-4-7, and 2-5-6 are clearly diamagnetic. (5-3-6 has not yet been obtained phase-pure.) The susceptibilities (in 10^{-4} emu/mol, corrected for core but not valence electron contributions), vary from –0.4 to –0.34, –2.53 to –2.48, and –0.61 to –0.71, respectively, between room temperature and 50 K. Below 50 K, the susceptibilities show small rises, probably because of minor paramagnetic impurities. The ac resistivities of Mg_3Sb_2, $Mg_{4.5}La_4Sb_7$, and $Mg_{1.7}La_{4.9}Sb_6$ at 35 MHz appear to be substantially temperature-independent between 290 and 150 K, except that the measured effect with Mg_3Sb_2 fell below the limit of instrument sensitivity below 230 K. The calculated room-temperature resistivities, probably good within a factor of 3, are 530, 50, and 85 $\mu\Omega$·cm, respectively. The 5-4-7 and 2-5-6 samples showed appreciable charging when studied by XPS, indicating that they were poorly conducting. Use of the signals from adventitious C(1s) in an attempt to correct for charging suggested a valence band edge for 5-4-7 $\simeq$ 1 eV below E_F and gave shifts to lower binding energy of roughly 1.6 and 0.7 eV for La $3d_{5/2}$ (relative to La_2O_3) and approximately 1.0 and 0.6 eV for Sb $3d_{5/2}$ (relative to the element) for the 5-4-7 and 2-5-6 samples, respectively.

These modest resistivities and their negligible temperature dependencies are at first glance a little surprising in light of the magnetic and XPS properties and the structural characteristics of the phases. In fact, they are quite plausible when it is recognized that LaSb itself is a semi-metal. The optical gap of LaSb is 0.7–0.8 eV, but the room-temperature resistivity is a very similar 113 $\mu\Omega$·cm,[21] and a semi-metal character is well established by de Haas–van Alpen effect measurements.[22] The source of the effect is clear from band calculations; states derived from metal t_{2g} plus Sb p(π) become bonding and fall below the valence band at X (along the crystallographic axes).[23] Two of three X points should be retained when we intergrow LaSb slabs with Mg_3Sb_2 and therefore semi-metallic characteristics. Such a behavior does not appear to conflict with the valence principles incorporated in Zintl–Klemm classifications.

These intergrowth structures can be categorized as linear homogeneous examples in the systematics developed by Parthé et al.[24] (more details by Grin' [25]). Intergrowth of n Mg_3Sb_2 slabs with m pairs of LaSb layers such that, as observed, one additional layer of La replaces Mg in the interface gives a homologous series with compositions $Mg_{3n-1}La_{m+1}Sb_{2n+m}$. An additional intergrowth requirement is electroneutrality. For those systems wherein only Mg vacancies occur, the products $Mg_{3n-1.5}La_{m+1}Sb_{2n+m}$ are observed for $n = 2$, $m = 2, 3$ (5-3-6 and 5-4-7, respectively). With x La vacancies in 2-5-6 ($n = 1$, $m = 4$), the formulation becomes $Mg_{3n-1.5+2x}La_{m+1-x}Sb_{2n+m}$. It would be interesting to attempt the substitution of tin on the antimony lattice to see whether the catio vacancies can be eliminated. We certainly have not exhausted the present ternary possibilities, either. There is at least one more phase with an unsolved quasi-rhombohedral structure ($c \sim 89$ Å), and shorter range intergrowth examples could become appreciable under the right conditions.

Our attempts to synthesize analogous $Mg_{4.5}Ln_4Sb_7$ phases with Ln = Pr, Nd, Gd, and Tb were surprisingly unsuccessful, yielding only Mg_3Sb_2 and LnSb as major phases. This may result from the diminished value of $a/\sqrt{2}$ for these LnSb phases (4.50 Å for PrSb[11]) relative to 4.60 Å for LaSb, $a = 4.56$ Å for Mg_3Sb_2, and 4.62 Å for the observed intergrown examples with lanthanum. In other words, strain precludes the intergrowth. The combination of Mg_3As_2 (high-temperature type, $a = 4.264$ Å) with CeAs or LuSb ($a/\sqrt{2} = 4.270$ or 4.283 Å) is a speculative possibility.

A survey of compounds nominally isostructural with Mg_3Sb_2 leads us back to the large family of ternaries belonging to the $CaAl_2Si_2$ structure type,[20] viz., with $Al_2Si_2^{2-}$ bilayers (isoelectronic with $Mg_2Sb_2^{2-}$) separated by Ca^{2+} in octahedral surroundings. Mewis et al.[26,27] have synthesized a large variety of ternary $A^{II}M_2Pn_2$ examples [M = Zn, Cd (Cu, Mn); A = Ae, Eu, Yb], especially for Pn = P, As. These may also be versatile in forming unexpected intergrowth structures (as amply demonstrated in this article), but perhaps the right experiments have not been carried out. Cation vacancies for charge compensation will probably be favored in the more polar bilayers like $Mg_2As_2^{2-}$ or $Mn_2As_2^{2-}$, and the

(21) Abdusalyamova, M. N.; Shokirov, H. S.; Rakhmatov, O. I. *J. Less-Common Met.* **1990**, *166*, 221.
(22) Kitazawa, H.; Suzuki, T.; Seva, M.; Ogura, I.; Yanase, A.; Hasegawa, A.; Kasuga, T. *J. Magn. Magn. Mater.* **1983**, *31–34*, 421.
(23) Hasegawa, A. *J. Phys. Soc. Jpn.* **1985**, *54*, 677.
(24) Parthé, E.; Chabot, B. A.; Cenzual, K. *Chimia* **1985**, *39*, 164.
(25) Grin', Y. N. In *Modern Perspectives in Inorganic Crystal Chemistry*; Parthé, E., Ed.; Kluwer Academic Publishers: Dordrecht, Holland, 1992; p. 77.
(26) Mewis, A. *Z. Naturforsch.* **1978**, *33B*, 606.
(27) Mahan, A.; Mewis, A. *Z. Naturforsch.* **1983**, *38B*, 1041 and references therein.

good match between the *a* dimensions reported for Mg_3As_2 (4.26 Å) and $CaMn_2As_2$ (4.24 Å)[2] with $a/\sqrt{2}$ for NdAs (4.21 Å) and CeAs (4.30 Å) encourages their investigation. Systematic synthetic investigations are apt to lead to a plethora of novel compounds in the burgeoning field of polar intermetallics, some of which will provide further tests of the drive to achieve closed-shell examples that is so frequently expressed in Zintl phases.

The relationship of the present findings to those in the wide array of intergrowth structure types seems to be small-to-nil if we limit ourselves to macroscopic phases in which intergrowth involves variable slabs of both parents that are both wider than a small interfacial region, twin boundary, or shear plane. The closest appear to be the remarkable Al_4C_3–*n*AlN results (ch^{2+n} type) where the carbide can be re-expressed in terms of Al_2C_2 (cubic ZnS) plus Al_2C (CaF_2^{-1}) portions.[28,29] Many other intergrowth systems have been studied primarily by electron diffraction[30] and, sometimes, by powder X-ray diffraction as well, e.g., La_2O_3 + ThO_2 (or equivalent)[31] and SrO + *n*$SrTiO_3$.[32]

Acknowledgment. We are indebted to J. Ostenson and D. Finnemore for the magnetic data, to J. W. Anderegg for the XPS examinations, and to J. Shinar for the use of the "Q" apparatus.

Supplementary Material Available: Tables of additional data collection and refinement information and anisotropic atom displacement parameters for Mg_3Sb_2, $Mg_{4.5}La_4Sn_7$, $Mg_{4.6}La_3Sb_6$, and $Mg_{1.7}La_{4.9}Sb_6$ (2 pages). Ordering information is given on any current masthead page.

(28) Jeffrey, G. A.; Wu, V. Y. *Acta Crystallogr.* **1963**, *16*, 559; **1966**, *20*, 538.
(29) Pearson, W. B. *The Crystal Chemistry and Physics of Metals and Alloys*; J. Wiley: New York, 1972; p 408.
(30) Gopalakrishnan, J.; Ramanan, A.; Rao, C. N. R.; Jefferson, D. A.; Smith, D. J. *J. Solid State Chem.* **1984**, *55*, 101.
(31) O'Keeffe, M.; Hyde, B. G. *Struct. Bonding* **1985**, *61*, 88.
(32) Tilley, R. J. D. *J. Solid State Chem.* **1977**, *21*, 293.